Layered Distribution of Charge Carriers in Organic Thin Film Transistors

Arian Shehu,[1,2] Santiago D. Quiroga,[1] Pasquale D'Angelo,[1] Cristiano Albonetti,[1] Francesco Borgatti,[1] Mauro Murgia,[1] Andrea Scorzoni,[2] Pablo Stoliar,[1] and Fabio Biscarini[1,*]

[1]*Consiglio Nazionale delle Ricerche-Istituto per lo Studio dei Materiali Nanostrutturati (ISMN), Via P. Gobetti 101, 40129 Bologna, Italy*

[2]*Università di Perugia-Dipartimento di Ingegneria Elettronica e dell'Informazione (DIEI), Via G. Duranti 93, I-06125 Perugia, Italy*

(Received 28 October 2009; published 16 June 2010)

Drain-source current in organic thin-film transistors has been monitored *in situ* and in real time during the deposition of pentacene. The current starts to flow when percolation of the first monolayer (ML) occurs and, depending on the deposition rate, saturates at a coverage in the range 2–7 MLs. The number of active layers contributing to the current and the spatial distribution of charge carriers are modulated by the growth mode. The thickness of the accumulation layer, represented by an effective Debye length, scales as the morphological correlation length. These results show that the effective Debye length is not just a material parameter, but depends on the multiscale morphology. Earlier controversial results can be unified within this framework.

DOI: 10.1103/PhysRevLett.104.246602 PACS numbers: 72.80.Le, 68.37.Ps, 68.55.A−, 72.20.Jv

In organic field-effect transistors (OFET) an organic semiconductor, either a single crystal or a thin film, forms the channel between the source-drain electrodes. OFETs exhibit linear and saturation regime in their characteristics as in MOSFETs [1]. Several studies carried out on conjugated molecules and oligomers thermally sublimed in high or ultrahigh vacuum (HV/UHV), have established that they behave as low-dimensional devices [2]. Charge transport for *p*-type OFETs, under hole accumulation regime, is confined within a few molecular layers on top of the gate dielectric. Experiments on sexithiophene FETs demonstrated that the first 2 monolayers (MLs) sustain the whole current [3]. Dihexylquaterthienyl FETs exhibited maxima in the hole mobility at 1 and 2 ML [4]. Experiments on pentacene evidenced a charge transport layer of 5–6 MLs or 1–2 MLs with an offset in the percolation threshold [5–7]. The reported variability of the effective channel thickness prompts the question on whether there is a framework which unifies these observations.

We start from the consideration that all these thin films are grown in out-of-equilibrium conditions and exhibit a stacked morphology. Despite the extensive effort in understanding growth using morphology scaling arguments [8–16], there is a limited knowledge on how the morphology is correlated to the charge transport [17,18].

In this Letter, we show that the FET response measured *in situ* and real time (during the growth of the semiconductor thin film) is a direct probe of the finer morphological details of the charge transport layer, which allows us to correlate the stacked morphology and the distribution of charge carriers in pentacene. By a systematic change of the deposition rate Φ we show that the effective Debye length varies from 2–5 MLs, and scales as the morphological correlation length. Counterintuitively, the charge carrier mobility remains constant.

Our *in situ* experiments are carried out on a home-built setup. We measure the drain-source current I_{DS} during the growth of pentacene thin-film avoiding device instabilities due to ambient exposure of the semiconductor [19–22]. We systematically vary the film morphology by means of Φ in the range 0.1–5 ML/ min with the substrate kept at room temperature [23–25]. Pentacene (Fluka) is thermally sublimed in HV (base pressure 2×10^{-6} mbar) on FET test patterns with channel lengths of 20 and 40 μm, and width 11 200 e 22 400 μm, respectively. Drain (*D*) and source (*S*) Au (150 nm)/Cr (3–5 nm) electrodes are lithographically defined on a 200 nm thick SiO_2 film thermally grown on highly doped *n*-type Si wafer which acts as common gate electrode. Before deposition, test patterns are cleaned with Piranha solution (1:1 H_2O_2 : H_2SO_4) for 15 min and in 4% HF solution for a few seconds. This procedure removes Cr at the boundary between the electrode and the channel [26,27]. I_{DS} is monitored in real-time at a fixed gate source voltage $V_{GS} = -40$ V and a drain-source voltage $V_{DS} = -1$ V. These conditions imply linear FET regime with I_{DS} scaling as the charge carrier mobility, and threshold voltage almost invariant (Fig. S1 in Ref. [28]). I_{DS} is measured on two FET structures every 200 ms. At least 4 devices are measured for each Φ. The film thickness, expressed as coverage Θ in ML (1 ML = 1.5 nm) is monitored with a calibrated quartz microbalance. At $\Theta =$ 7 ML the deposition is stopped and *in situ* FET electrical characterization is performed on each device (Figs. S2–3 in Ref. [28]). No hysteresis is observed in the transfer characteristics of all measured devices. The thin-film morphology of each device at $\Theta = 7$ ML is analyzed *ex situ* with atomic force microscopy (AFM).

In Figs. 1(a)–1(d) the current I_{DS} (normalized to its value at $\Theta = 7$ ML) vs Θ is shown for different Φ. Each curve is the average on all devices measured *in situ* for each

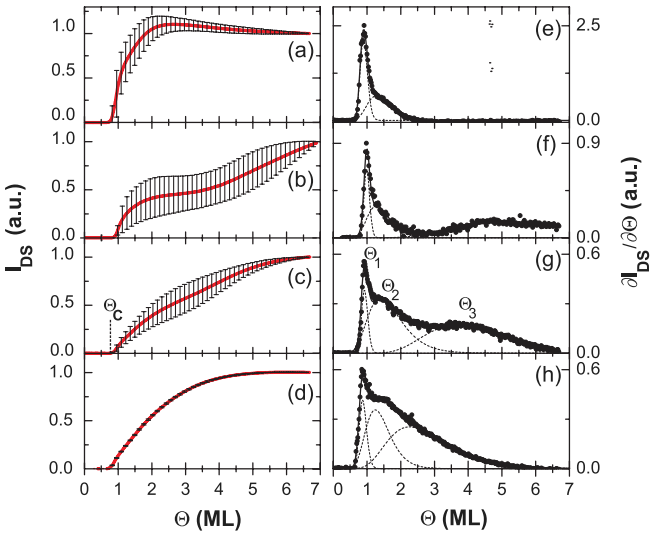

FIG. 1 (color online). Left: Evolution of I_{DS} (normalized to $\Theta = 7$ ML) vs Θ measured in real time and *in situ* conditions for Φ: (a) 0.1 ML/min, (b) 0.2 ML/min, (c) 1 ML/min, (d) 5 ML/min. The percolation threshold Θ_c is schematically indicated (dotted vertical segment on curve (c)). Error bars are standard deviations. Right: derivative $\partial I_{DS}/\partial\Theta$ (e–h, circles); continuous line is best-fit by linear combination of three log-normal functions (dotted lines).

Φ. Initially I_{DS} rises as $(\Theta - \Theta_c)^{\nu}$ [29,30]. The critical coverage Θ_c marks the appearance of the first connected percolation path between drain and source. Θ_c and ν values are plotted in Fig. 2. Θ_c decreases logarithmically from 0.80 to 0.67 ML, approaching the 2D value ≈ 0.5 as Φ increases. The values for ν are above 1.5 at lower rates, and below at higher rates. Theory would interpret this evidence as a change in dimensionality of percolation from 3D to 2D for increasing Φ. These values are also in agreement with previous ones reported in literature and appear consistent with the analysis of nucleation and growth of pentacene [3,4,25].

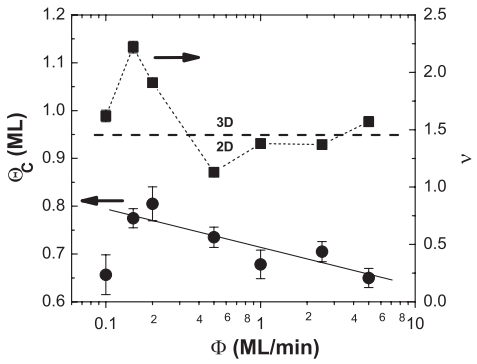

FIG. 2. Dependence of the percolation threshold Θ_c (circles) and the exponent ν (squares) vs Φ. Solid line is best fit with Θ_c (ML) $= 0.71–0.08 \cdot \log[\Phi/(\mathrm{ML/min})]$. Dotted line is a guide to the eye. Dashed line refers to ν and marks the transition between percolation in two and three dimensions.

The saturation thickness Θ_{SAT} of I_{DS} is clearly rate dependent. For $\Phi = 0.1$ ML/min [Fig. 1(a)] I_{DS} reaches a maximum at 2 ML, then it decreases. This indicates that charge carriers flow in the first two molecular layers next to the dielectric, in agreement with the findings on oligothienyls and pentacene [3,4,7]. The decrease of I_{DS} above 2 ML can be due to bias stress and/or polarization of the upper incomplete layers, which can slow down or trap charge carriers [31]. For $\Phi > 0.1$ ML/min, $\Theta_{\mathrm{SAT}} > 2$ ML. At $\Phi = 1$ ML/min [Fig. 1(c)], $\Theta_{\mathrm{SAT}} \approx 6$ ML which is consistent with other observations on pentacene *ex situ* and *in situ* [5,6]. In this range of Φ, Θ_{SAT} shifts towards lower values approaching to 3 ML with the increase of Φ. Since increasing Φ yields an enhancement of the layer-by-layer character of the growth mode, this trend reflects a correlation between the apparent thickness of the transport layer and the formation of a percolation path in the layers above 2 ML. The detailed features (maximum, inflection points and plateau) of I_{DS} curves in Figs. 1(a)–1(d) exhibit a coherent evolution vs Φ. We analyze them through the derivative $\partial I_{DS}/\partial\Theta$ shown in Figs. 1(e)–1(h) Such a quantity scales as the charge carrier density when the charge mobility is independent of the charge carrier density. Since this is not the case in organic semiconductors, it contains also the weight of the percolation conductivity [32]. $\partial I_{DS}/\partial\Theta$ exhibits a non monotonic decay with multiple peaks. Each peak position represents the nominal coverage at which the charge carrier population is maximum and percolates across the channel.

In order to quantify the position and the width of the observed peaks, each $\partial I_{DS}/\partial\Theta$ curve is fitted with a linear combination of log-normal functions [33]: $y_{\mathrm{fit}}(\Theta) = (2\pi)^{-1/2}\sum_n w_n \sigma_n^{-1}\Theta^{-1}\exp(-[\ln(\Theta/\Theta_n)]^2/2\sigma_n^2)$, with $n = 1, 2, 3$. Here Θ_n is the central value, $\exp(\sigma_n)$ the standard deviation, w_n is the statistical weight estimated by the area under the curve. This basis set yields estimated parameter errors always below 5%. In Fig. 3(a), the peak position Θ_n of the nth layer ($n = 1, 2, 3$) is plotted as a function of Φ. The first peak Θ_1 is centered at 1 ML and is narrow for all Φ. This is an indication that the first ML completes before the second nucleates on top. The second peak occurs at $\Theta_2 = 1.5–2$ ML, its width changing slowly with Φ. This indicates that also the second layer grows layer-by-layer, although islands in the upper layers start nucleating before completion. The position of the third peak Θ_3 decays monotonically from 6 to 3 ML as $\Theta_3 \approx \Phi^{-\gamma}$ with $\gamma = 0.25 \pm 0.02$. The width of Θ_3 is broader than that of both the first and second peak, and scales as $\Phi^{-\delta}$ with $\delta = 0.23 \pm 0.03$. This indicates that the film changes its growth mode from a layer-plus-island mode (Stranski-Krastanov-like with stacking of progressively smaller monolayer terraces) at low Φ to a quasi layer-by-layer mode at the higher Φ. At $\Phi = 0.1$ ML/min there are only two peaks and the derivative vanishes at 2 MLs. The absence of the third peak indicates that the islands above

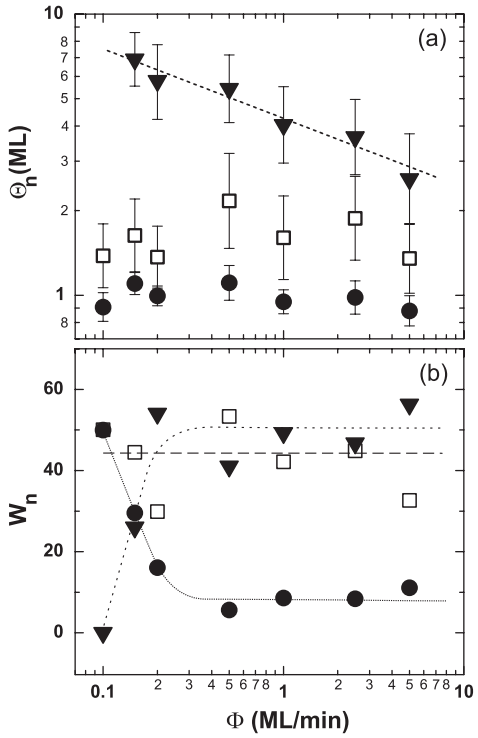

FIG. 3. (a) Position of the nth peak Θ_n with $n = 1$ (circles), 2 (squares), 3 (triangles) vs Φ. Dashed line is the power law fit $\Theta_3 \approx \Phi^{-\gamma}$ with $\gamma = 0.25 \pm 0.02$; (b) corresponding populations w_n vs Φ. Lines are guides to the eye.

the second monolayer are effectively disconnected, and a percolation pathway between drain and source is not formed.

The relative contributions of the different layers can be modulated by means of Φ. Figure 3(b) shows the best-fit populations w_n viz. the fractional contribution of each layer to I_{DS}. At $\Phi = 0.1$ ML/min, the contributions of the first and second layers are comparable. This, together with the large percolation threshold $\Theta_c > 0.8$ ML (Fig. 2), points to the nucleation and growth of two monolayer thick islands. Indeed, ideal 2D percolation threshold is 0.5 ML. The maximum at 2 ML in Fig. 1(a) corresponds to the filling of the first bilayer. In the Θ range explored the third peak is not observed, although it may appear above 7 ML (extrapolation of the dashed curve in Fig. 3(a) points to 8 ML). For $\Phi > 0.1$ ML/min, the contribution of the first layer decreases rapidly to 10% of the overall current, whereas the contributions of the second and third layer become dominant. This proves that the third layer is active in charge transport, provided its percolation threshold is achieved.

The curves in Figs. 1(e)–1(h) do not decay exponentially. Continuum models based on semi-infinite and isotropic semiconductors predict that the screening depth (Debye length) of the gate electric field penetrating the organic semiconductor is less than 1 nm [34,35]. In pentacene OFETs this would imply that the accumulation layer will be confined in the first monolayer and the first monolayer will sustain the whole drain-source current. Our experimental evidence shows that the first monolayer sustain only a small fraction of the drain-source current and the whole current is transported by completion of three monolayers. We define an effective Debye length L_D as the thickness corresponding to 63% of the saturation current. Hence it is not strictly a material parameter, but is related to the growth mode. We also identify the peak at the largest thickness, i.e., either Θ_2 or Θ_3, as the apparent channel thickness. The derivative $\partial I_{DS}/\partial\Theta$ vanishes approximately at $\Theta_{SAT} \approx \Theta_3 \cdot \exp(\sigma_3)$ for $\Phi > 0.1$ ML/min. The plot of Θ_{SAT} and L_D is shown in Fig. 4(a). The effective Debye length scales from $\Theta = 4.9$ ML to $\Theta = 2.2$ ML following the trend of Θ_{SAT} vs Φ. Thus 63% of the charge carriers resides in the first 3 ML, except for the case $\Phi = 0.1$ ML/min where only 2 ML are active. This suggests that the Debye length in thin-film organic semiconductors should be reconsidered for understanding charge transport in anisotropic layers.

Owing to the sensitivity of the *in situ* measurement to the growth mode, we can correlate L_D and Θ_{SAT} to morphological length scales. Pentacene film morphology is shown in Fig. 4(b). The monolayer stacks form interconnected

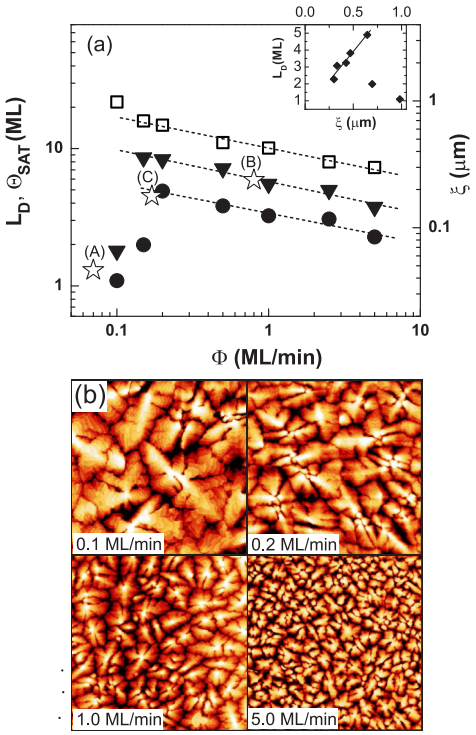

FIG. 4 (color online). (a) Left axis: Θ_{SAT} (triangles) and effective Debye length L_D (circles); Right axis: correlation length ξ (squares) vs deposition rate Φ. The dashed lines are power law fits for $\Phi > 0.15$ ML/min. Stars (A), (B), and (C) are the values from Refs. [5–7]. Inset: Correlation plot between L_D and ξ; solid line is the fit $L_D = 0.43 + 6.97 \cdot \xi$. (b) 5×5 μm^2 AFM images in the FET channel at $\Theta = 7$ ML.

islands giving rise to a self-affine dendritic morphology. The characteristic island size decreases vs Φ. For interconnected islands, it is estimated as the correlation length ξ of the topographical fluctuations from the power spectrum density of AFM images [8]. Figure 4(a) shows that ξ obeys a power law $\xi \approx \Phi^{-\beta}$ with the exponent $\beta = 0.24 \pm 0.02$. The island number density scales as $\xi^{-2} \approx \Phi^{0.5}$, in agreement with earlier results on pentacene growth on SiO_2 surfaces [10,14]. Interestingly, ξ, Θ_{SAT} and L_D exhibit the same scaling exponent vs Φ. In the inset of Fig. 4(a) we show that the correlation between L_D and ξ is positive when growth is mostly 2D, whereas is negative when the growth becomes more 3D. This demonstrates that the domain size can improve or worsen charge transport depending on the growth mode. It also implies that optimum terrace stacking consists of islands with comparable lateral size. We find that the FET mobility, measured *in situ* on 7 ML films, remains constant at $\mu = 0.14 \pm 0.03$ $cm^2/V\,s$ [28]. This counterintuitive result suggests that the domain boundaries of the dendritic islands are major barriers to transport [36].

The discrepancy among earlier reports of Θ_{SAT} on pentacene is settled when the reported values are renormalized with respect to the growth mode [37]. In Fig. 4(a) we show that the values (stars) from Refs. [5–7] vs their Φ superimpose onto our experimental curve [38].

In conclusion, we demonstrated that *in situ* and real-time electrical measurements are sensitive to the finer details of the growth of the semiconductor film. New physical insights of charge transport in OFETs has been shown, viz., the charge carriers distribute across a variable number of layers depending on the stacking morphology, leading to a variation of the effective Debye length from 2–5 ML. This framework reconciliates earlier results that were apparently at variance. The charge carrier distribution across the layered architecture prompts for new description of charge transport accounting for the correlations within the stacks and the anisotropy, and not just material parameters.

We would like to thank C. Zannoni for useful discussions. This work is supported by EC FP7 ONE-P Large Scale Project No. 212311.

*f.biscarini@bo.ismn.cnr.it

[1] G. Horowitz, Adv. Mater. **10**, 365 (1998).
[2] A. Dodalabapur, L. Torsi, and H. E. Katz, Science **268**, 270 (1995).
[3] F. Dinelli *et al.*, Phys. Rev. Lett. **92**, 116802 (2004).
[4] T. Muck *et al.*, Synth. Met. **146**, 317 (2004).
[5] M. Kiguchi *et al.*, Phys. Rev. B **71**, 035332 (2005).
[6] R. Ruiz *et al.*, Adv. Mater. **17**, 1795 (2005).
[7] B. N. Park, S. Seo, and P. G. Evans, J. Phys. D **40**, 3506 (2007).
[8] F. Biscarini *et al.*, Phys. Rev. B **52**, 14 868 (1995); Phys. Rev. Lett. **78**, 2389 (1997).
[9] P. Fenter *et al.*, Phys. Rev. B **56**, 3046 (1997).
[10] F.-J. Meyer zu Heringdorf, M. C. Reuter, and R. M. Tromp, Nature (London) **412**, 517 (2001).
[11] M. Brinkmann *et al.*, Phys. Rev. B **61**, R16 339 (2000); M. Brinkmann, S. Graff, and F. Biscarini, *ibid.* **66**, 165430 (2002).
[12] R. Ruiz *et al.*, Phys. Rev. Lett. **91**, 136102 (2003); Phys. Rev. B **67**, 125406 (2003).
[13] R. Ruiz *et al.*, Chem. Mater. **16**, 4497 (2004).
[14] S. Pratontep *et al.*, Phys. Rev. B **69**, 165201 (2004); Synth. Met. **146**, 387 (2004).
[15] A. C. Mayer *et al.*, Phys. Rev. B **73**, 205307 (2006).
[16] S. Hong *et al.*, Appl. Phys. Lett. **92**, 253304 (2008).
[17] H. Yanagisawa *et al.*, Thin Solid Films **464–465**, 398 (2004).
[18] C. Kim, A. Facchetti, and T. J. Marks, Science **318**, 76 (2007).
[19] M. Matters *et al.*, Synth. Met. **102**, 998 (1999).
[20] H. L. Gomes *et al.*, Appl. Phys. Lett. **88**, 082101 (2006).
[21] S. G. J. Mathijssen *et al.*, Adv. Mater. **19**, 2785 (2007).
[22] P. D'Angelo *et al.*, Appl. Phys. A **95**, 55 (2009).
[23] J. A. Venables, G. D. T. Spiller, and M. Hanbücken, Rep. Prog. Phys. **47**, 399 (1984).
[24] P. Stoliar *et al.*, J. Am. Chem. Soc. **129**, 6477 (2007).
[25] S. Verlaak *et al.*, Phys. Rev. B **68**, 195409 (2003).
[26] K. R. Williams *et al.*, J. Microelectromech. Syst. **12**, 761 (2003).
[27] S. G. J. Mathijssen *et al.*, Nature Nanotech. **4**, 674 (2009).
[28] See supplementary material at http://link.aps.org/supplemental/10.1103/PhysRevLett.104.246602 for supporting information on electrical characteristics.
[29] S. Kirkpatrick, Rev. Mod. Phys. **45**, 574 (1973); M. Sahimi, J. Phys. A **17**, L601 (1984).
[30] D. Stauffer and A. Aharony, *Introduction to Percolation Theory* (CRC Press, London, 1994).
[31] T. Cramer *et al.*, Phys. Rev. B **79**, 155316 (2009).
[32] P. W. M. Blom and M. C. J. M. Vissenberg, Phys. Rev. Lett. **80**, 3819 (1998); C. Tanase *et al.*, Org. Electron. **4**, 33 (2003).
[33] M. Abramowitz and I. A. Stegun, *Handbook of Mathematical Functions with Formulas, Graphs, and Mathematical Tables* (Dover Publications, New York, NY, 1972).
[34] G. Horowitz, J. Mater. Res. **19**, 1946 (2004).
[35] M. Mottaghi and G. Horowitz, Org. Electron. **7**, 528 (2006).
[36] P. Annibale *et al.*, J. Phys. Chem. A **111**, 12 854 (2007).
[37] A.-L. Barabasi and H. E. Stanley, *Fractal Concepts in Surface Growth* (Cambridge University Press, Cambridge, England, 1995).
[38] In Ref. [7] $\Theta_{SAT} \approx$ 1–2 MLs; however Fig. 6 reveals that 2 ML is an inflection point and the current still increases above 4 MLs.